ACS APPLIED ELECTRONIC MATERIALS

pubs.acs.org/acsaelm Article

Femtosecond Laser-Processed Perovskite Thin Films with Reduced Nonradiative Recombination and Improved Photodetecting Performance

Xuhang Chen, Tao Huang, Ruiyan Li, Yucai Lin, Jianjun Yang, Wei Li,* and Weili Yu*

Cite This: *ACS Appl. Electron. Mater.* 2023, 5, 3316−3323 Read Online

ACCESS | Metrics & More | Article Recommendations | Supporting Information

ABSTRACT: Carrier recombination plays a key role in determining the performance of perovskite devices, wherein nonradiative recombination hinders carrier extraction and limits the performance of perovskite-based optoelectronic devices (e.g., solar cells and photodetectors). To reduce nonradiative recombination, passivating the surface and grain boundary defects with chemicals has been extensively studied. However, this method has limitations such as pollution, complicated procedures, etc. Here, we provide a physical approach to reduce the nonradiative recombination loss of $MAPbI_3$ perovskite thin films using femtosecond (fs) laser processing. Perovskite thin films processed by fs laser show an enhanced photoluminescence (PL) intensity, extended lifetime, smaller grain size, smooth surface, and improved photodetector performance. The effect of laser processing is attributed to a decrease in the number of trap centers per grain and polished perovskite surface, which act as nonradiative recombination centers in the perovskite thin films. This research provides a promising way to improve the performance of perovskite optoelectronic devices.

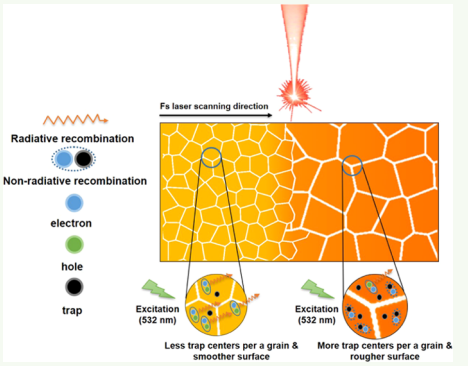

KEYWORDS: *perovskite, femtosecond laser, nonradiative recombination, grain size, photodetector*

INTRODUCTION

In the past decade, perovskites have been increasingly studied since Kojima et al. first used all-organic perovskites to fabricate solar cells and achieved a power conversion efficiency (PCE) of 3.81%.[1] So far, various perovskites have been used to fabricate various optoelectronic devices, such as solar cells, photodetectors, light-emitting diodes (LED), lasers, and phototransistors, due to their excellent photoelectric properties.[1−7] To enhance the performance of the devices, one key challenge is to reduce nonradiative recombination caused by surface and grain boundary defects.[8] One of the promising approaches is to passivate the surface defects of perovskite thin films with chemicals,[9−14] such as organic small molecules,[9] polymers,[10] inorganic molecules,[11] etc. The traditional chemical surface passivation method improves the performance of perovskite optoelectronic devices, but it also has limitations, including a complicated perovskite manufacturing process, reduced conductivity of perovskites, and potential environmental pollution. Therefore, in addition to the above methods, a promising method to reduce nonradiative recombination is needed.

Recently, some researchers tried applying femtosecond (fs) laser to process perovskite materials,[15−18] as clean ablation can be caused by fs laser without having unwanted secondary effects due to the suppression of thermal diffusion.[19,20] This method utilized a much shorter pulse duration of fs laser than the electron−lattice energy relaxation time, thus giving rise to a significant nonequilibrium state between electrons and lattices.[16,18] For instance, Kong et al. used fs laser to polish the perovskite surface to enhance the performance of perovskite solar cells.[16] Xing et al. applied fs laser to induce micro-/nanostructures on the surface of perovskite single crystals to improve their photoluminescence (PL).[21] Liang et al. achieved high-quality patterning of perovskite films for LED through fs laser ablation.[17] Arciniegas et al. grew locally perovskite nano- and microcrystals induced by fs laser.[22] Very recently, Sun et al. reported three-dimensional (3D) direct lithography of stable perovskite nanocrystals in glass with ultrafast laser-induced liquid nanophase separation.[23] However, there are few studies on the application of femtosecond laser processing to reduce the nonradiative recombination decay of perovskite films without severe ablation of perovskite films. More studies on the mechanism of the laser-processing effect are still needed.

Here, we irradiated the surface of a $MAPbI_3$ perovskite film using a femtosecond laser with optimized parameters (laser power density and scanning speed), thereby changing the morphology of the film on a glass substrate and its physical

Received: March 18, 2023
Accepted: May 2, 2023
Published: May 15, 2023

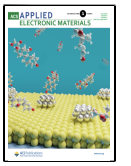

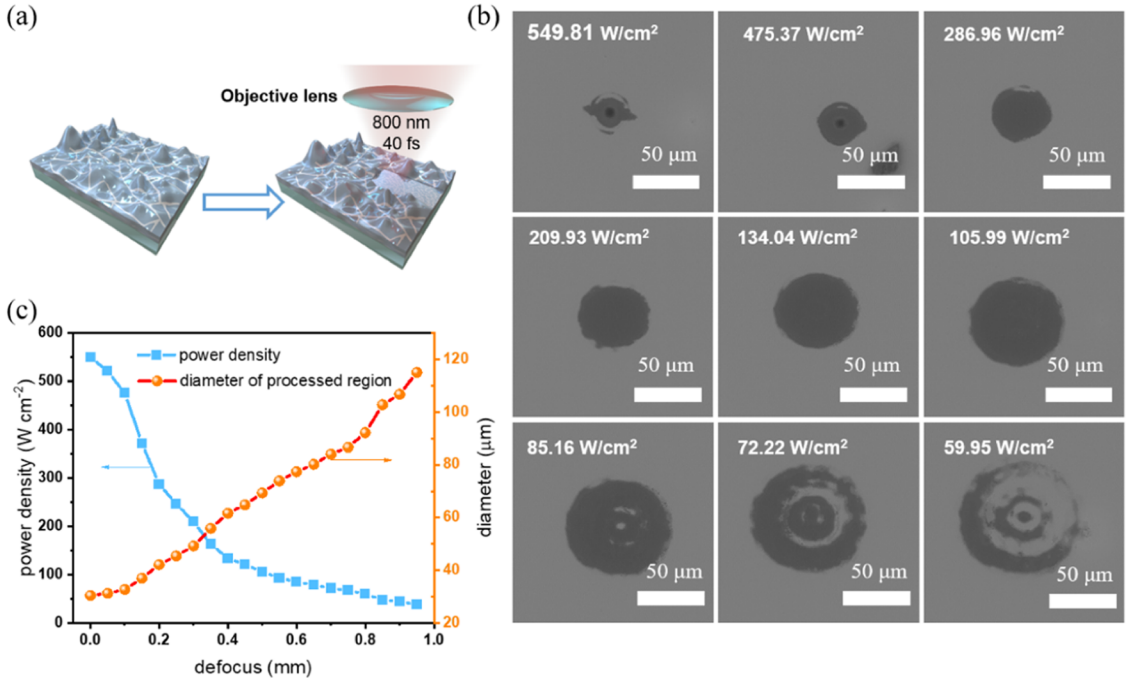

Figure 1. (a) Schematic diagram of the experimental process of laser-processed $MAPbI_3$ thin films. (b) SEM images of the processed $MAPbI_3$ thin films with varying power densities. The ablated hole is marked in Figure S2a. (c) Curves depicting the relationships between the defocus distance, power density, and diameter of the processed region.

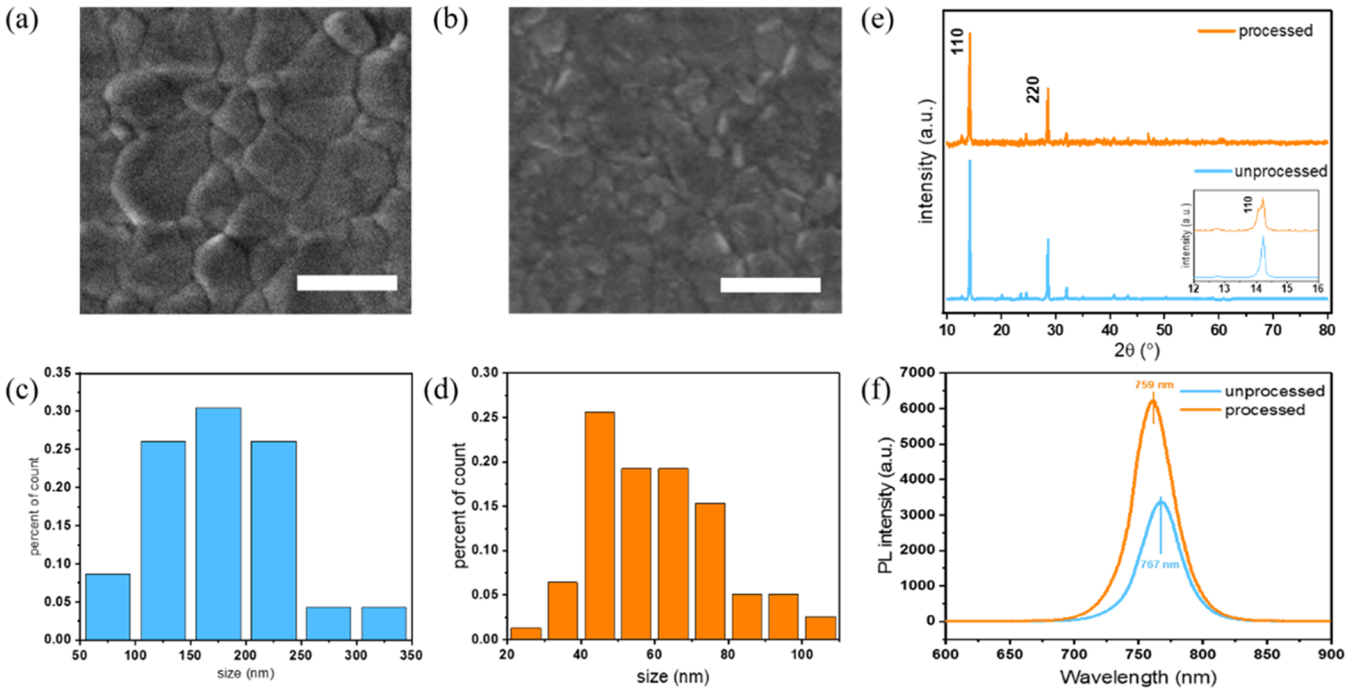

Figure 2. Comparison of SEM images of (a) UMTFs and (b) PMTFs with nanocrystals formed, reducing the average grain size. The number of grains with different grain sizes for (c) UMTFs and (d) PMTFs. (e) XRD patterns of UMTFs and PMTFs. (f) PL spectra of UMTFs and PMTFs with 532 nm laser excitation. The scale bars are 300 nm.

properties. As a result, we observed that both the average size of perovskite grains and the surface roughness of the perovskite surface were reduced, which contributes to the reduction of nonradiative recombination sites and enhancement of the carrier lifetime. Finally, we used the resulting films to fabricate photodetectors and improved their performance. This work provides a physical method to reduce the nonradiative recombination of perovskite thin films without complicated perovskite fabrication processes and potential environmental pollution.

RESULTS AND DISCUSSION

Figure 1a presents a schematic diagram of this experimental process, and the fs laser optical path is displayed in Figure S1. We

https://doi.org/10.1021/acsaelm.3c00357
ACS Appl. Electron. Mater. 2023, 5, 3316−3323

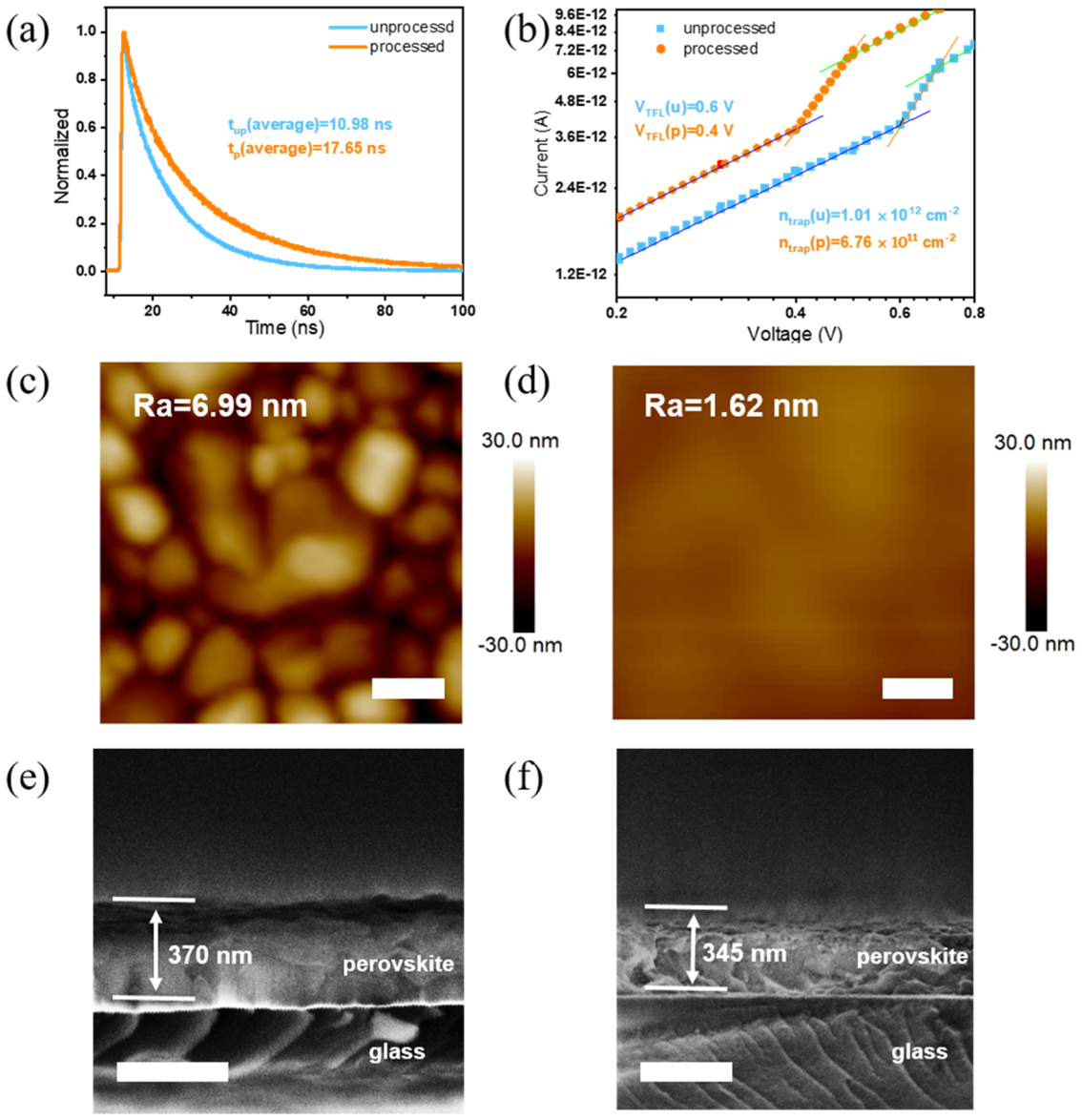

Figure 3. (a) TRPL spectra of UMTFs and PMTFs with 532 nm laser excitation. (b) SCLC curves of UMTFs and PMTFs. Comparison of AFM images of (c) UMTFs and (d) PMTFs. The scale bars are 200 nm. Cross-sectional SEM images of (e) UMTFs and (f) PMTFs. The scale bars are 400 nm.

prepared the perovskite precursor by dissolving MAI and PbI_2 with a molar proportion of 1:1 in a solvent mixture of *N*,*N*-dimethylformamide (DMF) and dimethyl sulfoxide (DMSO). One-step spin-coating was adopted to fabricate $MAPbI_3$ thin films on glass substrates.[24] Next, we applied an 800 nm laser with a 40 fs pulse duration to scan $MAPbI_3$ thin-film surfaces, where an ultrafast reaction between the laser and the perovskite occurred.[25] We adjusted the defocus distance (the distance before the focus, *D*) to investigate the influence of the laser power density on perovskite thin films. Scanning electron microscopy (SEM) images of the resultant thin films with different defocus distances are presented in Figure 1b, which shows that the ablated hole disappears when *D* is 0.2 mm (286.96 W cm^{-2}) due to the lower laser power density. Nevertheless, the diffraction phenomenon of the processed region becomes more severe with the laser power density decreasing from 0 mm (549.81 W cm^{-2}) to 0.8 mm (59.95 W cm^{-2}) continuously. The relationships between the *D* value, power density, and diameter of the processed region are depicted in Figure 1c. The appropriate defocus distance of 0.75 mm (67.90 W cm^{-2}) without an ablated hole and severe diffraction phenomenon was chosen here, as shown in Figure S2b. Furthermore, we adjusted the range of the laser scanning velocity (v) from 0.005 to 0.03 mm s^{-1}, and their confocal microscopy images are displayed in Figure S3. It is found that the higher the speed, the more severe the diffraction phenomenon, the worse the processing effect, and the more uneven the processing area. The best homogeneity was achieved when v was 0.005 mm s^{-1} (the minimum velocity of the 3D mobile platform used in this experiment), and so we chose this velocity to process perovskite thin films.

To explore the influence of laser processing on the optical and structural properties of $MAPbI_3$ thin films and reveal its mechanism, we performed SEM, X-ray diffraction (XRD), and PL spectroscopy of the unprocessed $MAPbI_3$ thin films (UMTFs) and processed $MAPbI_3$ thin films (PMTFs), as shown in Figure 2. SEM images of a UMTF and PMTF displayed in Figure 2a,b, respectively, show the abundantly

https://doi.org/10.1021/acsaelm.3c00357
ACS Appl. Electron. Mater. 2023, 5, 3316−3323

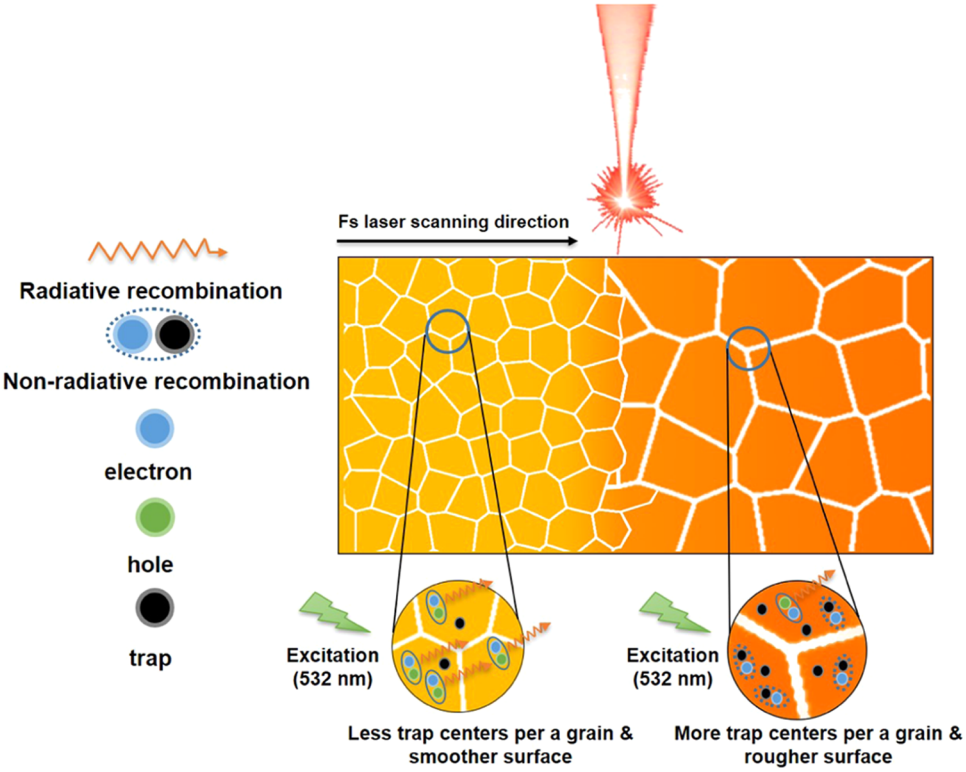

Figure 4. Schematic illustrating the morphology of a fs laser-processed perovskite film and its effects on the reduced nonradiative recombination. Laser scanning from left to right shows a smaller grain size in the processed region (left region) than that in the unprocessed region (right region). The enlarged view at the bottom shows the lower number of traps per grain and thus less nonradiative recombination at the processed region. The smooth surface (left region) is indicated by yellow color, and the rough surface (right) is indicated by orange color.

formed nanocrystals and the narrower grain boundaries achieved by PMTF. These small crystals were formed by the recrystallization of grains subjected to laser-induced melting, decreasing the number of individual trap centers in bulk or on the surface of grains (rather than dangling bonds on the surface), which are responsible for nonradiative recombination in metal halide perovskites.[26] Figure 2c,d shows the grain sizes of UMTFs and PMTFs extracted from SEM images, where the average grain size of PMTFs is 60.64 nm, less than that of UMTFs (177.18 nm). Besides, no drastic changes are found in the composition of the $MAPbI_3$ surface after laser processing from the results of the energy-dispersive spectrum (EDS), as shown in Figures S4 and S5. This indicates that fs laser with optimized parameters can process $MAPbI_3$ thin films without damaging the components of the films. In addition, XRD spectra of UMTFs and PMTFs are shown in Figure 2e, which revealed that no apparent change of the crystal facets occurred after laser processing. The magnified XRD pattern in the range of 12−16° is presented in the inset of Figure 2e, which shows the smaller crystal grain size in PMTFs than in UMTFs due to the larger full width at half-maximum (FWHM). The results further support the conclusions made from SEM images. Figure 2f shows the PL spectra of PMTFs and UMTFs excited by a 532 nm laser, from which we can observe a blue shift of the peak, indicating the increasing band gap of perovskites. As previously reported, the spontaneous radiative recombination between shallow trap states leads to a red shift of the PL spectra.[27,28] Thus, the blue shift of the PL peak is due to an increase in the energy of the shallow trap states. Besides, the absorption spectra of PMTFs and UMTFs are shown in Figure S6, which also present a blue shift of the absorption spectra. Consequently, we ascribed the increasing band gap to the reduced shallow trap states on the surface. More importantly, we discovered that the PL intensity was enhanced. As previously reported, the lesser the number of traps per grain, the higher the photoluminescence quantum yield (PLQY) of a film for materials with well-passivated surfaces and hindered excitation transport between grains through simple statistical analysis.[26] Therefore, by reducing the grain size through laser processing, the available bulk traps between a larger number of grains were redistributed to decrease the number of traps per grain, thus improving the PLQY and ultimately reducing nonradiative recombination sites in the grain bulk.

To further shed light on the laser-reduced nonradiative recombination, we further compared the photophysical properties of PMTFs and UMTFs. We measured the time-resolved photoluminescence (TRPL) spectra of PMTFs and UMTFs, as displayed in Figure 3a, which uncovered the carrier lifetime of these samples. Using the biexponential fit and the detailed fitting parameters shown in Table S1, the lifetime of PMTFs is calculated to be 17.65 ns, which is higher than that of UMTFs of 10.98 ns, indicating that nonradiative recombination can be suppressed for PMTFs.[29] In order to investigate the trap density (n_{trap}) of both PMTFs and UMTFs, we conducted a space-charge-limited current (SCLC) measurement, as shown in Figure 3b, which shows a trap-filled limit voltage (V_{TFL}) of PMTFs of 0.4 V, which is lower than that of UMTFs of 0.6 V. As we know, V_{TFL} is the applied voltage at the kink point, and so we further calculated the trap density of both thin films by the following equation[30]

https://doi.org/10.1021/acsaelm.3c00357
ACS Appl. Electron. Mater. 2023, 5, 3316−3323

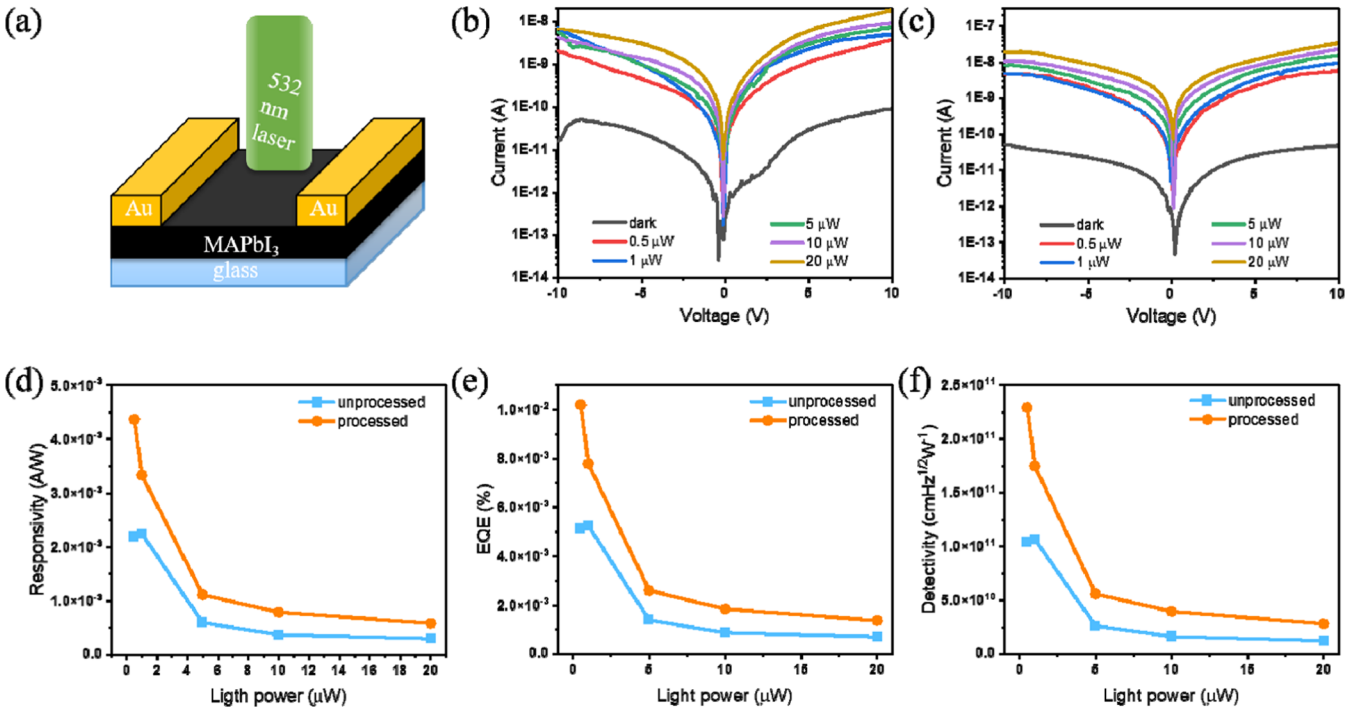

Figure 5. (a) Lateral structure of photodetectors with two Au electrodes. *I*−*V* curves of (b) UMTFs and (c) PMTFs under dark and 532 nm light illumination with various light intensities, respectively. (d) Responsivity, (e) EQE, and (f) detectivity as a function of incident light intensity for UMTFs and PMTFs, respectively.

$$V_{\mathrm{TEL}} = \frac{\pi e n_{\mathrm{trap}} d}{4\varepsilon_0 \varepsilon} \tag{1}$$

where d is the gap width between two adjacent Au electrodes, ε_0 is the vacuum permittivity, and ε is the relative dielectric constant for $MAPbI_3$. Therefore, the calculated values of n_{trap} are 5.07×10^{11} and 3.38×10^{11} cm^{-2}, respectively, which confirms that PMTFs have a lower n_{trap} than UMTFs. The atomic force microscopy (AFM) images are displayed in Figure 3c,d, which present the morphology and roughness of UMTFs and PMTFs, respectively. The roughness of UMTFs is found to be 6.99 nm from the AFM image, which is higher than that of PMTFs (1.62 nm). The reduced roughness of the laser-processed perovskite films indicated that the surface of the $MAPbI_3$ thin film was polished and became smoother. Besides, the cross-sectional SEM images in Figure 3e,f also show a thickness of PMTFs of 345 nm, which is thinner than that of UMTFs, i.e., 370 nm. The 3D AFM images presented in Figure S7 show the thinner and smoother profile of PMFTs, which further supports the above conclusion. As previously reported, the smooth surface has better contact between the perovskite layer and other functional layers (such as hole-transport layers, electron-transport layers, and electrodes).[31] Consequently, the perovskite with a smoother surface after fs laser processing contributes to a decreased possibility of nonradiative recombination as the light-absorbing layer of devices. The morphological changes of fs laser-processed perovskite thin films and their effect on nonradiative recombination are illustrated in Figure 4. The enlarged view at the bottom shows grains with a smaller average size in the left region than that in the right region, which contributes to reducing the number of trap centers per grain, thus leading to less nonradiative recombination. Besides, the roughness of the surface of the left region (smooth surface is indicated with yellow color) is lower than that of the right region (rough surface is indicated with orange color).

Finally, given that $MAPbI_3$ thin films with fewer nonradiative recombination sites were obtained, we fabricated photodetector devices using PMTFs and UMTFs as light-absorbing layers with a lateral structure by thermally evaporating Au electrodes on the top, as shown in Figure 5a. Then, we measured the device photocurrents under dark and light illumination of a 532 nm laser, and the corresponding *I*−*V* curves are shown in Figure 5b,c, respectively. It is noted that the PMTF-based devices present larger photocurrents than UMTF-based devices. To evaluate the performance of the photodetectors, we calculated the three key parameters for characterization, including responsivity (R), external quantum efficiency (EQE), and detectivity (D). R is defined as the photocurrent stimulated by a single unit light in a single unit area, which is calculated by the following equation[32]

$$R = \frac{I_{\mathrm{light}} - I_{\mathrm{dark}}}{P_{\mathrm{in}}} \tag{2}$$

Here I_{light}, I_{dark}, and P_{in} are the photocurrent, dark current, and incident optical power intensity, respectively. The diameter of the light-illuminated spot is 18.91 μm, which is smaller than the 20 μm width of the effective working area of the devices, and so the incident optical power intensity is equal to the power intensity accepted by the effective working area of the devices. EQE is the ratio of the number of excitation electrons to incident photons expressed by the following equation[33]

$$\mathrm{EQE} = \frac{Rh\nu}{e} \tag{3}$$

Here, R is the responsivity, h represents Planck's constant, ν is the frequency of incident light, and e is the electronic charge. D is defined as the sensitivity of the devices under various noises; the

https://doi.org/10.1021/acsaelm.3c00357
ACS Appl. Electron. Mater. 2023, 5, 3316−3323

dark current is mainly affected by short noise in our test conditions, and thus, D is expressed by the following equation[34]

$$D = \frac{R}{\sqrt{2eJ_{\text{dark}}^{\ 2}}} \tag{4}$$

Here, J_{dark} is the dark current density of the photodetectors. Under a low bias of 5 V, PMTF-based photodetectors exhibit better performance, with an R of 3.33×10^{-3} A W^{-1}, EQE of 0.78%, and D of 1.75×10^{11} Jones at a light intensity of 1 μW. In contrast, the control UMTF-based photodetectors exhibit limited performance, with R, EQE, and D values evaluated to be 2.25×10^{-3} A W^{-1}, 0.53%, and 1.07×10^{11} Jones, respectively, as shown in Figure 5d–f. Besides, the response rates of PMTF- and UMTF-based devices are shown in Figure S8, which show rise and decay times for PMTF-based devices of 1.75 and 0.35 s, respectively, which are lower than those of 2.79 and 0.7 s for UMTF-based devices. A higher photocurrent is obtained for PMTF-based devices. The improved performance of PMTF-based devices is attributed to the reduced nonradiative recombination sites in perovskite thin films due to laser processing.

CONCLUSIONS

In summary, we demonstrated a promising strategy, which utilizes a femtosecond laser to process perovskite thin films and achieves reduced nonradiative recombination loss. Reduced grain size, enhanced PL, and altered roughness are also achieved. The mechanism of the reduced nonradiative recombination decay is discussed. It is found that laser processing decreases the number of trap centers per grain in bulk and makes the perovskite surface smoother, which helps reduce nonradiative recombination sites in bulk and on the surface. Finally, perovskite films with reduced nonradiative recombination sites are used as light-absorbing layers to fabricate photodetectors, and enhanced performance is achieved. This work provides a physical approach to reduce the nonradiative recombination loss of perovskite thin films with convenient perovskite fabrication processes, well-maintained perovskite conductibility, and environmental friendliness.

METHODS

Materials. Methylamine solution (40% aqueous solution) and hydriodic acid (HI, 95%) were both purchased from Aladdin company. Lead iodide (PbI_2, ≥99%) was obtained from Xi'an Polymer Light Technology Corp. Both *N*,*N*-dimethylformamide (DMF, 99.8%) and dimethyl sulfoxide (DMSO, ≥99.9%) were bought from Sigma-Aldrich. Toluene was bought from Chengdu Kelong Chemical Company. Methylammonium iodide (MAI) was synthesized by a previously reported method,[35] where a mixed solution of methylamine solution and HI (1:1, molar ratio) was stirred at 0 °C for 2 h. Then, rotary evaporation was used to remove the solvent to obtain a white powder at 60 °C, which was followed by redissolving the white powder (MAI) with anhydrous ethanol and recrystallizing it with anhydrous ether. This step was repeated three times. Finally, the white powder was filtered and dried at 60 °C in a vacuum for one night to obtain MAI.

Fabrication of $MAPbI_3$ Thin Films and Femtosecond Laser Processing. Here, we prepared the $MAPbI_3$ perovskite precursor with MAI (1 M) and PbI_2 (1 M) dissolved in mixed solvents of DMF and DMSO (7:3 volume ratio), followed by heating on a hotplate at 65 °C for 6 h, and obtained the transparent pure precursor. We obtained $MAPbI_3$ thin films through a one-step method here. We first cleaned the glass substrates successively with deionized water, ethanol, acetone, and isopropanol for 15 min individually by ultrasonication and dried them with nitrogen (N_2), which then were placed in UV–O_2 for hydrophilic treatment. Next, we spin-coated the perovskite precursor on the substrate at 500 and 2000 rpm for 5 and 60 s, respectively, and dripped 200 μL of toluene antisolvent after spin-coating for 25 s. Then, we transferred them onto a hotplate, followed by annealing at 65 °C for 1 min and 100 °C for 2 min. The fs laser processing of perovskite thin films was conducted under conditions of scanning velocity v = 0.005 mm s^{-1} and defocus distance D = 0.75 mm (peak power density 67.90 W cm^{-2}).

Femtosecond Laser System. A linearly polarized 40 fs laser with a central wavelength of 800 nm was used here at a repetition rate of 1 kHz, which was excited by a chirped pulse amplification of a Ti:sapphire laser system (Spitfire Ace, Spectra Physics). We adjusted the parameters of the defocus distance and scanning speed under a laser power of 4 mW to investigate the effects of interaction between the laser and perovskite thin films.

Characterization. SEM images were obtained using Phenom Prox FiberMetric and Zeiss Auriga-45-06 instruments. EDS was performed using an X-Max detector (Oxford Instruments). We obtained confocal microscopy images using a VK-X250K microscope. We characterized the crystal structure by X-ray diffraction with a Bruker D8 Focus instrument. A HORIBA Scientific Raman Spectrometer was applied to obtain PL spectra at 532 nm in air. The TRPL spectra were obtained using a MicroTime 200 time-resolved fluorescence microscope (PicoQuant) excited by a 532 nm laser at room temperature in air. The roughness of the thin films was measured using a Keyence laser confocal microscope (VK-X1000).

Lateral Photodetector Fabrication. Au electrodes with 80 nm thickness and a 20 μm channel were thermally evaporated on the crystal surface to fabricate a lateral photodetector and measure their SCLC. The electrodes were 290 μm long and 55 μm wide. A Keithley 4200A semiconductor parametric analyzer (Tektronix) and a C-100 probe station from TPSi-Company were used to obtain the I–V curves at room temperature in air. We measured the photoresponse of the devices using a 532 nm laser with a tuning power intensity from 0.5 to 20 μW.

ASSOCIATED CONTENT

Supporting Information

The Supporting Information is available free of charge at https://pubs.acs.org/doi/10.1021/acsaelm.3c00357.

Optical path of fs laser processing; SEM images of perovskite films treated by defocus distances of 0 and 0.75 mm; confocal images of perovskite films treated at various scanning speeds; EDS of UMTFs and PMTFs; absorption spectra of UMTFs and PMTFs; 3D AFM images of UMTFs and PMTFs; response rates of UMTFs and PMTFs; TRPL fitting data (PDF)

AUTHOR INFORMATION

Corresponding Authors

Wei Li – *GPL Photonics Laboratory, State Key Laboratory of Luminescence and Applications, Changchun Institute of Optics, Fine Mechanics and Physics, Chinese Academy of Sciences, Changchun 130033, P. R. China; University of Chinese Academy of Sciences, Beijing 100049, P. R. China;* orcid.org/0000-0002-2227-9431; Email: weili1@ciomp.ac.cn

Weili Yu – *GPL Photonics Laboratory, State Key Laboratory of Luminescence and Applications, Changchun Institute of Optics, Fine Mechanics and Physics, Chinese Academy of Sciences, Changchun 130033, P. R. China; University of Chinese Academy of Sciences, Beijing 100049, P. R. China;* orcid.org/0000-0001-5075-9638; Email: weili.yu@ciomp.ac.cn

https://doi.org/10.1021/acsaelm.3c00357
ACS Appl. Electron. Mater. 2023, 5, 3316–3323

Authors

Xuhang Chen − *GPL Photonics Laboratory, State Key Laboratory of Luminescence and Applications, Changchun Institute of Optics, Fine Mechanics and Physics, Chinese Academy of Sciences, Changchun 130033, P. R. China; University of Chinese Academy of Sciences, Beijing 100049, P. R. China*

Tao Huang − *GPL Photonics Laboratory, State Key Laboratory of Luminescence and Applications, Changchun Institute of Optics, Fine Mechanics and Physics, Chinese Academy of Sciences, Changchun 130033, P. R. China; University of Chinese Academy of Sciences, Beijing 100049, P. R. China*

Ruiyan Li − *GPL Photonics Laboratory, State Key Laboratory of Luminescence and Applications, Changchun Institute of Optics, Fine Mechanics and Physics, Chinese Academy of Sciences, Changchun 130033, P. R. China; University of Chinese Academy of Sciences, Beijing 100049, P. R. China*

Yucai Lin − *GPL Photonics Laboratory, State Key Laboratory of Luminescence and Applications, Changchun Institute of Optics, Fine Mechanics and Physics, Chinese Academy of Sciences, Changchun 130033, P. R. China; University of Chinese Academy of Sciences, Beijing 100049, P. R. China;* orcid.org/0000-0002-7466-5094

Jianjun Yang − *GPL Photonics Laboratory, State Key Laboratory of Luminescence and Applications, Changchun Institute of Optics, Fine Mechanics and Physics, Chinese Academy of Sciences, Changchun 130033, P. R. China; University of Chinese Academy of Sciences, Beijing 100049, P. R. China*

Complete contact information is available at: https://pubs.acs.org/10.1021/acsaelm.3c00357

Notes

The authors declare no competing financial interest.

■ ACKNOWLEDGMENTS

W.L. acknowledges financial support from the National Science Foundation of China (NSFC, 62134009 and 62121005) and W.Y. acknowledges financial support from the Natural Science Foundation of Jilin Province (20220101203JC).

■ REFERENCES

(1) Kojima, A.; Teshima, K.; Shirai, Y.; Miyasaka, T. Organometal Halide Perovskites as Visible-Light Sensitizers for Photovoltaic Cells. *J. Am. Chem. Soc.* **2009**, *131*, 6050−6051.

(2) Min, H.; Lee, D. Y.; Kim, J.; Kim, G.; Lee, K. S.; Kim, J.; Paik, M. J.; Kim, Y. K.; Kim, K. S.; Kim, M. G.; Shin, T. J.; Seok, S. I. Perovskite solar cells with atomically coherent interlayers on SnO_2 electrodes. *Nature* **2021**, *598*, 444−450.

(3) Gao, Y.; Liu, Y.; Zhang, F.; Bao, X.; Xu, Z.; Bai, X.; Lu, M.; Wu, Y.; Wu, Z.; Zhang, Y.; Wang, Q.; Gao, X.; Wang, Y.; Shi, Z.; Hu, J.; Yu, W. W.; Zhang, Y. High-Performance Perovskite Light-Emitting Diodes Enabled by Passivating Defect and Constructing Dual Energy-Transfer Pathway through Functional Perovskite Nanocrystals. *Adv. Mater.* **2022**, *34*, No. 2207445.

(4) Qin, C.; Sandanayaka, A. S. D.; Zhao, C.; Matsushima, T.; Zhang, D.; Fujihara, T.; Adachi, C. Stable room-temperature continuous-wave lasing in quasi-2D perovskite films. *Nature* **2020**, *585*, 53−57.

(5) Zou, Y.; Li, F.; Zhao, C.; Xing, J.; Yu, Z.; Yu, W.; Guo, C. Anomalous Ambipolar Phototransistors Based on All-Inorganic $CsPbBr_3$ Perovskite at Room Temperature. *Adv. Opt. Mater.* **2019**, *7*, No. 1900676.

(6) Huang, T.; Zhu, Z.; Zhao, C.; Kong, W.; Chen, X.; Li, R.; Yu, Z.; Shi, Z.; Li, D.; Yang, B.; Yu, W. Enhancing two-dimensional perovskite photodetector performance through balancing carrier density and directional transport. *J. Mater. Chem. A* **2022**, *10*, 21044−21052.

(7) Yu, W.; Li, F.; Huang, T.; Li, W.; Wu, T. Go beyond the limit: Rationally designed mixed-dimensional perovskite/semiconductor heterostructures and their applications. *Innovation* **2023**, *4*, No. 100363.

(8) De Quilettes, D. W.; Vorpahl, S. M.; Stranks, S. D.; Nagaoka, H.; Eperon, G. E.; Ziffer, M. E.; Snaith, H. J.; Ginger, D. S. Impact of microstructure on local carrier lifetime in perovskite solar cells. *Science* **2015**, *348*, 683−686.

(9) Yoon, H.; Kang, S. M.; Lee, J.-K.; Choi, M. Hysteresis-free low-temperature-processed planar perovskite solar cells with 19.1% efficiency. *Energy Environ. Sci.* **2016**, *9*, 2262−2266.

(10) Han, T.-H.; Lee, J.-W.; Choi, C.; Tan, S.; Lee, C.; Zhao, Y.; Dai, Z.; De Marco, N.; Lee, S.-J.; Bae, S.-H.; Yuan, Y.; Lee, H. M.; Huang, Y.; Yang, Y. Perovskite-polymer composite cross-linker approach for highly-stable and efficient perovskite solar cells. *Nat. Commun.* **2019**, *10*, No. 520.

(11) Liu, S.-C.; Li, Z.; Yang, Y.; Wang, X.; Chen, Y.-X.; Xue, D.-J.; Hu, J.-S. Investigation of Oxygen Passivation for High-Performance All-Inorganic Perovskite Solar Cells. *J. Am. Chem. Soc.* **2019**, *141*, 18075−18082.

(12) Seo, J.; Park, S.; Chan Kim, Y.; Jeon, N. J.; Noh, J. H.; Yoon, S. C.; Seok, S. I. Benefits of very thin PCBM and LiF layers for solution-processed p−i−n perovskite solar cells. *Energy Environ. Sci.* **2014**, *7*, 2642−2646.

(13) Mohd Yusoff, A. R. B.; Vasilopoulou, M.; Georgiadou, D. G.; Palilis, L. C.; Abate, A.; Nazeeruddin, M. K. Passivation and process engineering approaches of halide perovskite films for high efficiency and stability perovskite solar cells. *Energy Environ. Sci.* **2021**, *14*, 2906−2953.

(14) Wang, H.; Wang, Z.; Yang, Z.; Xu, Y.; Ding, Y.; Tan, L.; Yi, C.; Zhang, Z.; Meng, K.; Chen, G.; Zhao, Y.; Luo, Y.; Zhang, X.; Hagfeldt, A.; Luo, J. Ligand-Modulated Excess PbI_2 Nanosheets for Highly Efficient and Stable Perovskite Solar Cells. *Adv. Mater.* **2020**, *32*, No. 2000865.

(15) Rajan, R. A.; Tao, H.; Yu, W.; Yang, J. Space-resolved light emitting and lasing behaviors of crystalline perovskites upon femtosecond laser ablation. *Mater. Today Phys.* **2023**, *31*, No. 101000.

(16) Kong, W.; Zhao, C.; Xing, J.; Zou, Y.; Huang, T.; Li, F.; Yang, J.; Yu, W.; Guo, C. Enhancing Perovskite Solar Cell Performance through Femtosecond Laser Polishing. *Solar RRL* **2020**, *4*, No. 2000189.

(17) Liang, S.-Y.; Liu, Y.-F.; Zhang, H.-J.; Ji, Z.-K.; Xia, H. High-Quality Patterning of $CsPbBr_3$ Perovskite Films through Lamination-Assisted Femtosecond Laser Ablation toward Light-Emitting Diodes. *ACS Appl. Mater. Interfaces* **2022**, *14*, 46958−46963.

(18) Jiang, L.; Wang, A.-D.; Li, B.; Cui, T.-H.; Lu, Y.-F. Electrons dynamics control by shaping femtosecond laser pulses in micro/nanofabrication: modeling, method, measurement and application. *Light: Sci. Appl.* **2018**, *7*, No. 17134.

(19) Stuart, B. C.; Feit, M. D.; Rubenchik, A. M.; Shore, B. W.; Perry, M. D. Laser-Induced Damage in Dielectrics with Nanosecond to Subpicosecond Pulses. *Phys. Rev. Lett.* **1995**, *74*, 2248−2251.

(20) Sugioka, K.; Cheng, Y. Ultrafast lasers—reliable tools for advanced materials processing. *Light: Sci. Appl.* **2014**, *3*, No. e149.

(21) Xing, J.; Zheng, X.; Yu, Z.; Lei, Y.; Hou, L.; Zou, Y.; Zhao, C.; Wang, B.; Yu, H.; Pan, D.; Zhai, Y.; Cheng, J.; Zhou, D.; Qu, S.; Yang, J.; Ganeev, R. A.; Yu, W.; Guo, C. Dramatically Enhanced Photoluminescence from Femtosecond Laser Induced Micro-/Nanostructures on $MAPbBr_3$ Single Crystal Surface. *Adv. Opt. Mater.* **2018**, *6*, No. 1800411.

(22) Arciniegas, M. P.; Castelli, A.; Piazza, S.; Dogan, S.; Ceseracciu, L.; Krahne, R.; Duocastella, M.; Manna, L. Laser-Induced Localized Growth of Methylammonium Lead Halide Perovskite Nano- and Microcrystals on Substrates. *Adv. Funct. Mater.* **2017**, *27*, No. 1701613.

(23) Sun, K.; Tan, D.; Fang, X.; Xia, X.; Lin, D.; Song, J.; Lin, Y.; Liu, Z.; Gu, M.; Yue, Y.; Qiu, J. Three-dimensional direct lithography of stable perovskite nanocrystals in glass. *Science* **2022**, *375*, 307−310.

(24) Ahn, N.; Son, D.-Y.; Jang, I.-H.; Kang, S. M.; Choi, M.; Park, N.-G. Highly Reproducible Perovskite Solar Cells with Average Efficiency of 18.3% and Best Efficiency of 19.7% Fabricated via Lewis Base Adduct of Lead(II) Iodide. *J. Am. Chem. Soc.* **2015**, *137*, 8696−8699.
(25) Malinauskas, M.; Žukauskas, A.; Hasegawa, S.; Hayasaki, Y.; Mizeikis, V.; Buividas, R.; Juodkazis, S. Ultrafast laser processing of materials: from science to industry. *Light: Sci. Appl.* **2016**, *5*, No. e16133.
(26) Scheblykin, I. G. Small Number of Defects per Nanostructure Leads to "Digital" Quenching of Photoluminescence: The Case of Metal Halide Perovskites. *Adv. Energy Mater.* **2020**, *10*, No. 2001724.
(27) Li, X.; Zhang, W.; Wang, Y.-C.; Zhang, W.; Wang, H.-Q.; Fang, J. In-situ cross-linking strategy for efficient and operationally stable methylammoniun lead iodide solar cells. *Nat. Commun.* **2018**, *9*, No. 3806.
(28) Shao, Y.; Xiao, Z.; Bi, C.; Yuan, Y.; Huang, J. Origin and elimination of photocurrent hysteresis by fullerene passivation in $CH_3NH_3PbI_3$ planar heterojunction solar cells. *Nat. Commun.* **2014**, *5*, No. 5784.
(29) Jiang, Q.; Zhao, Y.; Zhang, X.; Yang, X.; Chen, Y.; Chu, Z.; Ye, Q.; Li, X.; Yin, Z.; You, J. Surface passivation of perovskite film for efficient solar cells. *Nat. Photonics* **2019**, *13*, 460−466.
(30) Liu, Y.; Yang, Z.; Cui, D.; Ren, X.; Sun, J.; Liu, X.; Zhang, J.; Wei, Q.; Fan, H.; Yu, F.; Zhang, X.; Zhao, C.; Liu, S. F. Two-Inch-Sized Perovskite $CH_3NH_3PbX_3$ (X = Cl, Br, I) Crystals: Growth and Characterization. *Adv. Mater.* **2015**, *27*, 5176−5183.
(31) Zhang, H.; Zhao, C.; Li, D.; Guo, H.; Liao, F.; Cao, W.; Niu, X.; Zhao, Y. Effects of substrate temperature on the crystallization process and properties of mixed-ion perovskite layers. *J. Mater. Chem. A* **2019**, *7*, 2804−2811.
(32) Liang, F. X.; Liang, L.; Zhao, X. Y.; Luo, L. B.; Liu, Y. H.; Tong, X. W.; Zhang, Z. X.; Huang, J. C. A. A Sensitive Broadband (UV−vis−NIR) Perovskite Photodetector Using Topological Insulator as Electrodes. *Adv. Opt. Mater.* **2018**, No. 1801392.
(33) Lv, Q.; Lian, Z.; He, W.; Sun, J.-L.; Li, Q.; Yan, Q. A universal top-down approach toward thickness-controllable perovskite single-crystalline thin films. *J. Mater. Chem. C* **2018**, *6*, 4464−4470.
(34) Fang, Y.; Dong, Q.; Shao, Y.; Yuan, Y.; Huang, J. Highly narrowband perovskite single-crystal photodetectors enabled by surface-charge recombination. *Nat. Photonics* **2015**, *9*, 679−686.
(35) Shi, D.; Adinolfi, V.; Comin, R.; Yuan, M.; Alarousu, E.; Buin, A.; Chen, Y.; Hoogland, S.; Rothenberger, A.; Katsiev, K.; Losovyj, Y.; Zhang, X.; Dowben, P. A.; Mohammed, O. F.; Sargent, E. H.; Bakr, O. M. Low trap-state density and long carrier diffusion in organolead trihalide perovskite single crystals. *Science* **2015**, *347*, 519−522.

https://doi.org/10.1021/acsaelm.3c00357
ACS Appl. Electron. Mater. 2023, 5, 3316−3323